Journal of Aerosol Science 47 (2012) 39–47

Contents lists available at SciVerse ScienceDirect

Journal of Aerosol Science

journal homepage: www.elsevier.com/locate/jaerosci

An eddy interaction model for particle deposition

Vivek Agnihotri [a,*], Ghader Ghorbaniasl [a], Sylvia Verbanck [b], Chris Lacor [a]

[a] Department of Mechanical Engineering, Vrije Universiteit Brussel, Pleinlaan 2, 1050 Brussels, Belgium
[b] Respiratory Division, University Hospital, Vrije Universiteit Brussel, Laarbeeklaan 101, 1090 Brussel, Belgium

ARTICLE INFO

Article history:
Received 28 October 2011
Received in revised form
9 December 2011
Accepted 17 December 2011
Available online 28 December 2011

Keywords:
Mouth–throat model
Eddy interaction model
Aerosol deposition
Micron particles
Correction functions
CFD

ABSTRACT

Deposition of mono-disperse aerosols is studied numerically on a simplified human upper airway model (UAM). This paper presents new correction functions for eddy interaction model (EIM) in an attempt to improve the accuracy of predicting aerosol deposition in the UAM. Based on an Euler-Lagrange methodology, the fluid phase is solved using RANS (Reynolds Averaged Navier Stokes equation) and employing low-Reynolds SST k-ω turbulence model. The particle phase is solved using Lagrangian approach and employing an EIM model. Mono-disperse particle sizes of 3 and 6 μm are considered for breathing rates of 30 and 60 L/min. The proposed method of correction functions to EIM ("helicity EIM") is compared to the classical EIM assuming isotropy ("isotropic EIM") and to the EIM incorporating correction functions of Wang & James (1999) ("Wang and James EIM"). All three EIM methods are validated against experimental data of deposition efficiencies reported for a 90° bend pipe and for the UAM. In the latter case, total as well as compartmental deposition efficiencies are used for validation purposes. In both geometries, the present approach ("helicity EIM") predicts the deposition efficiency better than the "isotropic EIM". The results obtained with "helicity EIM" are of similar accuracy compared to those of "Wang and James EIM". Considering that the "helicity EIM" does not require the estimation of y^+ for each case, we suggest that this could be the preferred EIM correction method for simulation of respirable range aerosol particle deposition in the mouth-throat.

1. Introduction

In recent years, numerical and experimental studies have been conducted to understand the deposition behavior of aerosol particles in the human upper airway, which in the context of the present work is composed of the oral cavity, pharynx, larynx and trachea (considering mouth breathing). The most widely used numerical method employed to simulate particle deposition is the eddy interaction model (EIM) (Graham & James, 1996; Graham, 1998; Zhang et al., 2002; Kleinstreuer & Zhang, 2003; Matida et al., 2004; Jayaraju et al., 2008; Sandeau et al., 2010; Verbanck et al., 2011). The major drawback of classical EIM is that it assumes fluctuating velocities to be isotropic, an assumption that is inappropriate, especially near the walls where there strong anisotropic turbulent structures develop (Kallio & Reeks, 1989). When EIM with isotropic velocity fluctuations was considered, resulting simulations largely overpredicted aerosol deposition especially for particle sizes in the range 1–5 μm, the so-called "respirable range" (Matida et al., 2000; Zhang et al., 2004). Hence, many authors have employed large eddy simulation (LES) in an attempt to obtain a more accurate prediction of aerosol deposition in the human upper airway (Matida et al., 2006; Jayaraju et al., 2008). While LES coupled with Lagrangian particle tracking indeed greatly improves the simulation of experimental deposition efficiency, the method is time consuming. Therefore, RANS together with an appropriate turbulence model and EIM still remains

* Correspondence to: Department of Mechanical Engineering, Fluid Mechanics and Thermodynamics Research Group, Triomflaan 43-Room TL43 050 Brussels, Belgium. Tel.: +32 2 6292399; fax: +32 2 6292880.
E-mail address: vivekgnhtr@gmail.com (V. Agnihotri).

0021-8502/$ - see front matter © 2011 Elsevier Ltd. All rights reserved.
doi:10.1016/j.jaerosci.2011.12.003

Nomenclature

c	constant
d_p	particle diameter, m
exp	exponential function
k	turbulent kinetic energy, m^2/s^2
min( )	minimum function
Re_p	particle Reynolds number
Stk	Stokes number
t	time, s
t_e	eddy life time, s
t_{int}	eddy interaction time, s
t_{cros}	eddy crossing time, s
u	fluid velocity, m/s
u_p	particle velocity, m/s
u_{rel}	relative velocity, m/s
x_p	particle position, m
y^+	wall distance

Greek Letters

ε	turbulent dissipation rate, m^2/s^3
τ_r	particle relaxation time, s
ω	vorticity vector
ζ	random number
μ	dynamic viscosity, Ns/m^2
ρ	fluid density, kg/m^3
ρ_p	particle density, kg/m^3

Subscripts

p	particle
rel	relative

Superscripts

$( )'$	fluctuations

the most widely used method. In order to overcome the drawbacks of classical EIM assuming isotropy, Wang & James (1999) have proposed correction functions for velocity fluctuations obtained by curve fitting the direct numerical simulation (DNS) duct flow data of Kim et al. (1987) and Mansour et al. (1988). As indicated by Wang and James these correction functions are valid for $y^+ < 80$. In addition, Wang & James (1999) pointed out that, these functions are applicable only for flows with a low Reynolds number against which they are calibrated. For example, Matida et al. (2004) calibrated the range of $y^+ \leq 20$ for a flow rate of 90 L/min and $y^+ \leq 1$ for a flow rate of 30 L/min. While such correction functions do improve the simulation of particle deposition compared to classical EIM assuming isotropy, the main shortcoming of this approach is that the correction functions were derived for ducted flow geometry. Finally, it critically depends on the wall distance, which is usually difficult to estimate in complex geometries such as the human upper airway. The main contribution of this work was to avoid these limitations using a generalized EIM methodology (further referred to as "helicity EIM"), which also incorporates anisotropy but without any a priori estimation of y^+.

The "helicity EIM" methodology was applied to two test geometries, (a) 90° bend pipe at Re=10,000, (b) human upper airway model with different flow rates at 30 L/min and 60 L/min. The calculated numerical results were compared against the experimental results of Pui et al. (1987) and Verbanck et al. (2011) for both test cases, respectively. The fluid phase and the particle phase were solved numerically using FLUENT 13.0 solver; the "helicity EIM" methodology was implemented in FLUENT 13.0 using user-defined functions.

2. Mathematical background

2.1. Euler–Lagrange modeling

The fluid phase is simulated by numerically solving time-averaged RANS equations employing SST k-ω turbulence model (Menter, 1994) with low-Re corrections; the mathematical formulation for turbulence modeling is not reiterated here. The choice of the turbulence model is based on its ability for better handling transitional flows as is the case in mouth–throat geometries compared to other widely used k-ε turbulence model (Matida et al., 2004; Zhang et al., 2005; Stapleton et al., 2000).

The particle phase is solved employing a Lagrangian approach. The volume fraction, defined as the ratio of volume occupied by all particles combined to that occupied by the fluid, is of the order of 1e-7. The particle density is also several orders of a magnitude greater for the particle than for the fluid. Under these conditions, the assumptions for modeling the particle phase are:

- one way coupling i.e. particles have negligible effect on the turbulence, based on the classification map given by Elghobashi (1994),
- no particle-particle interaction, no particle rotation, no lift force,
- the only force to be taken into account is drag force,
- particles are considered perfect sphere,
- slip correction factor=1.

Based on the above assumptions, the equation for the motion of a single particle reads

$$\frac{d\boldsymbol{u}_p}{dt} = (\boldsymbol{u} - \boldsymbol{u}_p)/\tau_r \tag{1}$$

with $d\boldsymbol{x}_p/dt = \boldsymbol{u}_p$. In this equation, $\boldsymbol{x}_p$ is the particle position vector, $\boldsymbol{u}_p$ the instantaneous particle velocity vector and $\boldsymbol{u}$ the instantaneous fluid phase velocity vector. The particle relaxation time is denoted by τ_r given by

$$\tau_r = \frac{4}{3}\frac{\rho_p d_p}{\rho |u_{rel}| C_d} \tag{2}$$

where C_d is the drag coefficient, $|u_{rel}|$ is the particle absolute relative velocity magnitude, ρ_p and ρ are the particle density and fluid phase density, respectively. The estimation of drag coefficient is based on correlations as mentioned below

$$C_d = a_1 + \frac{a_2}{\mathrm{Re}_p} + \frac{a_3}{\mathrm{Re}_p^2} \tag{3}$$

where Re_p is the particle Reynolds number and coefficients a_i (i=1, 2, 3) are constants as given by Morsi & Alexander (1972). Using an implicit Euler discretization scheme, one obtains the particle velocity at time level $n+1$ as follows:

$$\boldsymbol{u}_p^{n+1} = \frac{\boldsymbol{u}_p^n + \boldsymbol{u}^n \Delta t/\tau_r}{1 + \Delta t/\tau_r} \tag{4}$$

In order to update the particle position, a trapezoidal discretization scheme is used. The relation for the particle position is given by

$$\boldsymbol{x}_p^{n+1} = \boldsymbol{x}_p^n + 0.5\Delta t(\boldsymbol{u}_p^{n+1} + \boldsymbol{u}_p^n) \tag{5}$$

It should be mentioned that the choice of the time-step depends upon the specification of the following parameters:

t_{cv}, the time required by the particle to cross a cell,
τ_r, particle relaxation time,
t_{int}, time spent by a particle within an eddy, which in turn depends upon the specification of the eddy parameters i.e. the eddy life time and the eddy length scale (eddy size).

Here, we have used the length scales and time scales as specified by Gosman & Ioannides (1981). This is expressed as below:

$$t_{\mathrm{int}} = \min(t_e, t_{cros}) \tag{6}$$

The terms t_e and t_{cros} denote the eddy life time and the eddy crossing time, respectively. One has

$$t_e = ck/e,$$
$$t_{cross} = -\tau_r \ln\left(1 - \frac{L_e}{\tau_r |u_{rel}|}\right) \tag{7}$$

where L_e denotes the eddy length scale. Taken together with ERCOFTAC best practices guidelines on dispersed multiphase flow (2000), the time step was chosen as $\min(t_{cv}, \tau_r, t_{\mathrm{int}})/5$.

2.2. EIM and correction functions

In the EIM, the effect of turbulence on the particle motion is introduced by decomposing $\boldsymbol{u}$ in Eq. (1) as $\overline{\boldsymbol{u}} + \xi \boldsymbol{u}'$, where $\overline{\boldsymbol{u}}$ is the mean flow velocity vector, ξ a Gaussian random number with zero mean and unit standard deviation and $\boldsymbol{u}'$ the fluctuation due to turbulence, which needs to be modeled. The turbulence fluctuation $\boldsymbol{u}'$ is obtained from the computed turbulent kinetic energy, k of the fluid-phase.

2.2.1. Isotropic EIM

In terms of Cartesian components, the velocity fluctuations are modeled as follows:

$$u' = v' = w' = \sqrt{\frac{2}{3}k} \tag{8}$$

As can be seen from Eq. (8), in modeling of the velocity fluctuations, an assumption of isotropy has been considered. In Cartesian component, the velocity fluctuation can then be expressed as:

$$u' = \xi\sqrt{\frac{2}{3}k}$$
$$v' = \xi\sqrt{\frac{2}{3}k}$$
$$w' = \xi\sqrt{\frac{2}{3}k} \tag{9}$$

2.2.2. Wang and James EIM

Wang & James (1999) introduced three correction functions namely f_u,f_v and f_w to account the anisotropic nature of the velocity fluctuations close to the wall. The correction functions f_u,f_v and f_w are, respectively, in the streamwise, wall normal and spanwise direction, and were obtained by curve fitting DNS data of Kim et al. (1987) and Mansour et al. (1988) as a function of y^+. The velocity fluctuations in Cartesian component form can again be expressed as below:

$$u' = f_u \xi \sqrt{\frac{2}{3}k}$$
$$v' = f_v \xi \sqrt{\frac{2}{3}k}$$
$$w' = f_w \xi \sqrt{\frac{2}{3}k} \tag{10}$$

where

$$f_u = 1 + 0.285(y^+ + 6)\exp(-0.455(y^+ + 6)^{0.53})$$
$$f_v = 1 - \exp(-0.02y^+)$$
$$f_w = \sqrt{3 - f_u^2 - f_v^2} \tag{11}$$

These correction functions are valid for $y^+ < 80$. As already mentioned by Wang & James (1999), the functions are applicable for flows with a low Reynolds number against which they are calibrated. For example, Matida et al. (2004) calibrated the range of $y^+ \leq 20$ for a flow rate of 90 L/min and ≤ 1 for a flow rate of 30 L/min.

2.2.3. Helicity EIM

The notion behind this EIM correction methodology has been proposed very recently by Ghorbaniasl et al. (submitted for publication), where the correction functions were used to estimate subgrid-scale stress coefficients. Even though the correction functions were meant for LES applications, in the present work, we use the same notion to account the anisotropic nature of turbulent velocity fluctuations close to the wall via helicity. In fact, it modifies the velocity fluctuations based on the flow field data obtained from RANS, considering that the velocity fluctuations should go to zero on the wall and in the region where the flow is laminar. In particular, the correction functions have the property of giving zero values, both in the laminar region and on the wall in each direction, as opposed to the damping functions introduced by Wang & James (1999) that give zero values only on the wall and in the wall normal direction. Since the correction functions $f_u$and f_w do not guarantee zero values on the wall for fluctuation velocity components of u', w' this can affect particle deposition characteristics close to the wall via Eq. (1). In general, it is believed that the deposition of particles on to the wall is mainly affected by the wall normal velocity fluctuation, as such there can be no observable differences in the particles cumulative deposition efficiency, but there can be differences in the local variation of particle deposition.

In the "helicity EIM", the correction functions do not depend on the estimation of the wall distance parameter (y^+). The flow field is only the input that is being used in these functions. Furthermore, the introduced functions are such that when they are applied to the velocity fluctuations, the turbulent kinetic energy k remains unchanged. We shall model the velocity fluctuations as follows:

$$u' = bG_x \xi \sqrt{\frac{2}{3}k}$$
$$v' = bG_y \xi \sqrt{\frac{2}{3}k}$$
$$w' = bG_z \xi \sqrt{\frac{2}{3}k} \tag{12}$$

In equation (12), bG_x, bG_y and bG_z are the correction functions, where from Ghorbaniasl et al., one has

$$G_x = \frac{0.5|H_x|}{\sqrt{H_x^2 + H_y^2 + H_z^2}}$$
$$G_y = \frac{0.5|H_y|}{\sqrt{H_x^2 + H_y^2 + H_z^2}}$$
$$G_z = \frac{0.5|H_z|}{\sqrt{H_x^2 + H_y^2 + H_z^2}} \tag{13}$$

Here, the value of the term b is set to be $2\sqrt{3}$ such that the computed turbulent kinetic energy remains unchanged. The terms H_x, H_y and H_z are evaluated as:

$$H_x = \omega_x u$$
$$H_y = \omega_y v$$
$$H_z = \omega_z w \tag{14}$$

and symbol $|\cdot|$ denotes the absolute value. In Eq. (14) u, v and w are the mean flow velocity components in x, y and z directions, respectively. The terms ω_x, ω_y and ω_z are the x-, y- and z-component of the vorticity vector, which are obtained by

$$\boldsymbol{\omega} = \nabla \times \boldsymbol{u} \tag{15}$$

Using these correction functions, zero values for velocity fluctuations are guaranteed on the walls and in laminar regions. As can be seen from Eqs. (12)–(15), the accuracy of the "helicity EIM" method in predicting near wall fluctuations depends on the accurate resolution of velocity field especially in the vicinity of the wall. As such it becomes important to have adequate cells near the wall so that the first cell adjacent to wall is in the viscous sub-layer, preferably the wall $y^+ \leq 1$.

3. Results and discussion

In this section, two test geometries are considered and the experimental data of aerosol deposition efficiency is compared with the results obtained by the classical EIM ("isotropic EIM"), the correction method proposed by Wang & James (1999) ("Wang and James EIM"), and the present methodology ("helicity EIM"). First, flow is simulated by employing RANS SST k-ω turbulence model and then particle trajectories are calculated as described in Section 2.

3.1. Test geometry 1—90° bend, Re=10,000

The computed deposition efficiencies are compared to the experimental results of Pui et al. (1987) for a 90° bend (Fig. 1) with a diameter, ϕ=8.51 mm and a radius of curvature, R_o=5.6 mm. The test geometry was discretized into 0.6 million hexahedral cells with a near wall clustering of elements with a stretching ratio of 1.1. The y^+ value of the first layer of cells next to the wall is about 1. The inlet section of the test bend has an entrance length, $l_e = 4.4 \times \phi \times \mathrm{Re}^{1/6}$ so as to have a fully developed turbulent velocity profile at the inlet.

In the experiments, it is assumed that Re=10,000 and Stokes number (Stk) varies in the range 0.25–1.35, where $Stk = C\rho_p d_p^2 U_{in}/18\mu r_\phi$ with C as a slip correction factor (considered=1, since in present simulations$d_p \gg 1\,\mu m$), ρ_p the particle density and d_p the particle diameter. Here, U_{in} is the inlet velocity magnitude, μ the dynamic viscosity and r_ϕ the tube radius. In the experiments, Pui et al. (1987) used oleic acid aerosols with air, where ρ_p/ρ=755 and ρ_p=895 kg/m^3. In the simulations, the same material properties are adopted and Stokes range of $0.05 \leq Stk \leq 1.5$ is considered.

Fig. 2 shows that the total deposition efficiency is overpredicted by "isotropic EIM", in particular for the Stk range below 0.5. By contrast, the total deposition efficiencies simulated by "Wang and James EIM" and the "helicity EIM" methods are in very good agreement with the experimental curve in the entire Stk range considered. Interestingly, the latter two methods also show a good agreement with the LES result of Breuer et al. (2006).

3.2. Test geometry 2—simplified human upper airway model

The CT based simplified UAM model is created by preserving all the critical geometrical features based on the work of Brouns et al. (2007) (Fig. 3a) with critical cross sections depicted in Fig. 3b. In addition to the total deposition, we also consider the particle deposition in four UAM compartments: (a) oral, (b) pharynx, (c) larynx, and (d) trachea (Fig. 3a).

The UAM model is discretized into 1.2 million hexahedral elements. Fig. 3b shows the mesh details of the discretization at different section planes with a near wall clustering of elements and a stretching ratio of 1.1. The y^+ value of the first layer of cells next to the wall is about 1.

For the total and the compartmental deposition efficiency in this particular UAM, experimental data exist for inspiration at a breathing rate of 30 L/min, and 60 L/min, and for 3 μm and 6 μm particles Verbanck et al. (2011). For

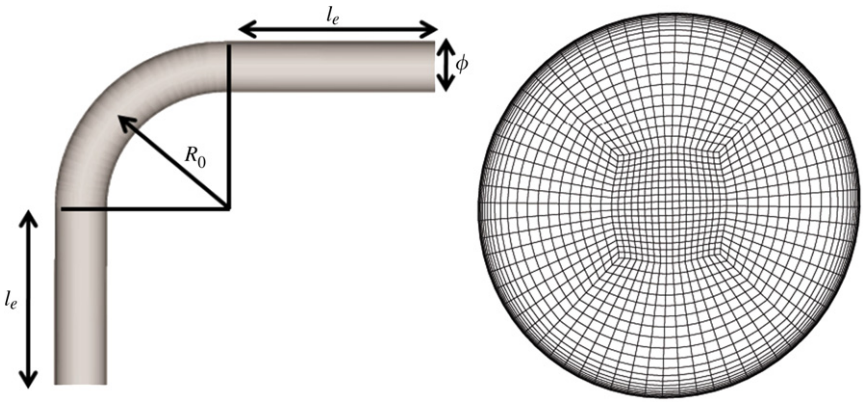

Fig. 1. 90° test bend. (left) Geometry details; (right) mesh cut plane at middle of the bend.

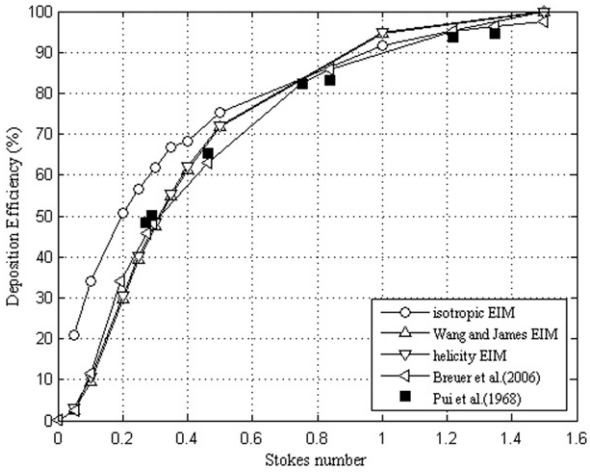

Fig. 2. Total deposition efficiency. (Connected symbols)—simulations; (disconnected symbols)—experiments.

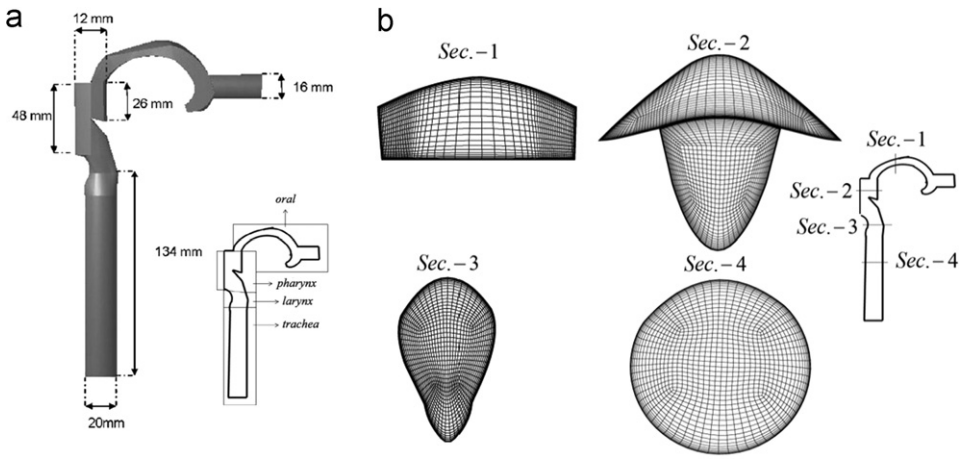

Fig. 3. (a) Simplified UAM model and respective compartments used in UAM. (b) Mesh at different section planes in UAM.

the simulations, the fluid-phase density and dynamic viscosity are set at $\rho = 1.2$ kg/m^3 and $\mu = 1.884\text{e}-5$ Ns/m^2, respectively. The particle density is set at $\rho_p = 912$ kg/m^3 with the particle diameter from 2–10 μm. In total, about 10,000 randomly distribution particles are injected at the inlet of the UAM model. Jayaraju et al. (2008) have reported that injecting 5000 or 15000 particles does not affect particle deposition.

Fig. 4 shows total deposition efficiency simulations for 30 L/min (left panel) and 60 L/min (right panel) as a function of $Stk \times \text{Re}^{0.37}$ as proposed by Grgic et al. (2004). Stokes (Stk) and Reynolds (Re) numbers are defined as:

$$Stk = \frac{\rho_p d_p^2 U_m}{18\mu d_m}$$
$$\text{Re} = \frac{\rho U_m d_m}{\mu} \tag{16}$$

where ρ and ρ_p are the fluid phase and particle density, d_m is the mean hydraulic diameter, U_m is the mean velocity and μ is the dynamic viscosity of the fluid phase. In Eq. (16), terms d_m and U_m are defined as:

$$d_m = 2\sqrt{\frac{V}{\pi L}}$$
$$U_m = \frac{Q}{LV} \tag{17}$$

where Q is the flow rate, L is mean cast length (in present case = 326 mm) and V is the cast volume (in present case = 90.6 mL). Compared with the empirical curve of Grgic et al. (2004) corresponding to a representative set of experimental data in different upper airway geometries, the "isotropic EIM" simulation largely overpredicts the total deposition over most of $Stk \times \text{Re}^{0.37}$ range. This is consistent with our previous studies (Jayaraju et al., 2008; Verbanck et al., 2011). The extent of overprediction for

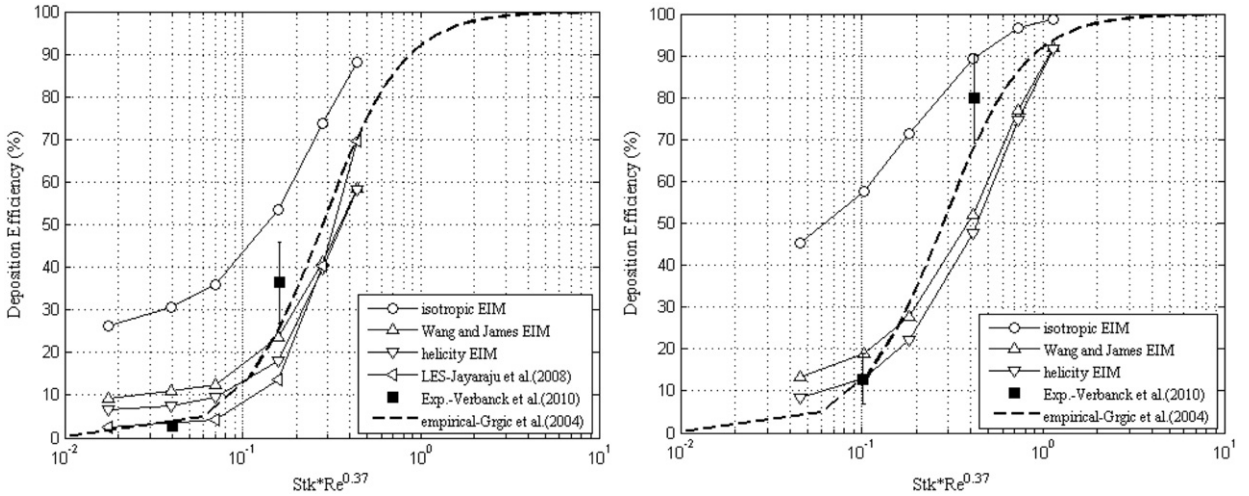

Fig. 4. Total deposition efficiencies: (left) 30 L/min and (right) 60 L/min; (connected symbols)—simulations; (disconnected symbols)—experiments.

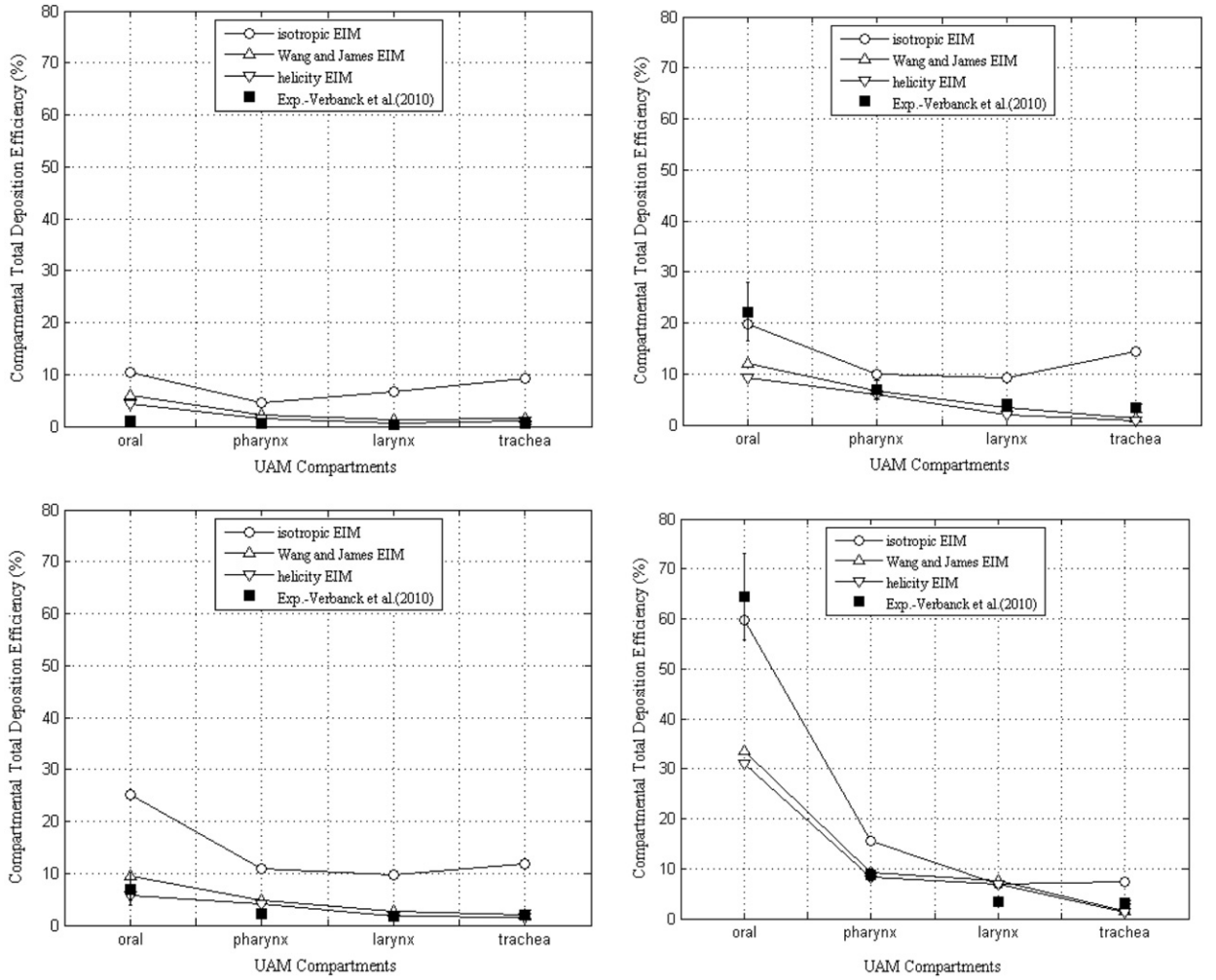

Fig. 5. Compartmental deposition efficiencies: (upper) 30 L/min and (lower) 60 L/min; (left) 3 μm and (right) 6μ m; (connected symbols)—simulations; (disconnected symbols)—experiments.

60 L/min is even greater than for 30 L/min for corresponding $Stk \times Re^{0.37}$ values. The "Wang and James EIM" and the "helicity EIM" method led to markedly lower total deposition values. In fact, in the $Stk \times Re^{0.37}$ range approaching 1, there is an underestimation with respect to the Grgic curve, and also with respect to experimental data obtained in the UAM. Alternatively, in the lowest $Stk \times Re^{0.37}$ range, simulations still slightly overpredict total deposition. We suspect that the implicit Euler time discretization scheme (first order accurate) could be responsible for this and we suggest that the effect of time marching scheme should be further investigated.

Fig. 5 shows the compartmental total deposition efficiencies for the flow rate of 30 L/min (upper panels) and 60 L/min (lower panels); the results for 3 μm are shown in the left panels, whereas those of 6 μm are illustrated in the right panels; all plots are scaled to the same range (0–80%) for direct comparison between all panels. The corresponding experimental data obtained by Verbanck et al. (2011) are also plotted in this figure for comparison. In Fig. 5, all deposition data correspond to the ratio of number of particles trapped in a given compartment to the total number of particles injected (instead of normalizing these to total deposition as was done in Verbanck et al., 2011). This representation enabled us to identify which compartments are responsible for the absolute differences observed in total deposition efficiencies (Fig. 4).

As can be seen, the overprediction of the "isotropic EIM" for the total deposition shown in Fig. 4 is also reflected in the compartmental deposition, and indeed so in all compartments for the smaller particle size (3 μm, left panel). However, for the bigger particle size (6 μm, right panels), the "isotropic EIM" produces oral deposition efficiencies that are closer to experimental values than do "Wang and James EIM" and the "helicity EIM". But in pharynx, larynx and trachea the compartmental deposition is simulated more accurately by "Wang and James EIM" and the "helicity EIM" methods, as compared to "isotropic EIM". At the lower flow rate and all particle sizes (upper panels), even though the "helicity EIM" and "Wang and James EIM" are closer to experiments compared to the "isotropic EIM", but still numerical discrepancies exist in the oral cavity. As can be seen from Fig. 5, there is an over prediction for the smaller particle size (left upper panel) and an underprediction for the bigger particle size (right upper panel). The numerical discrepancies associated with the "Wang and James EIM" and the proposed "helicity EIM" could be caused by the quality of the flow field solution in the vicinity of the wall. This in turn depends upon the turbulence model used and the grid resolution or as previously mentioned it could be because of implicit Euler time discretization used for updating particle velocity. In the case of "Wang and James EIM", it can also come from the correction functions used, which obtained from the DNS of channel flow. In general, this cannot be valid in the present UAM geometry.

Taken together, total and compartmental deposition efficiencies in the UAM are simulated more accurately by the "helicity EIM" and "Wang and James EIM" methods. The advantage of the "helicity EIM" in comparison with "Wang and James EIM" is that it is general and does not require any estimation of y^+.

4. Conclusion

In the framework of RANS coupled with EIM for studying the particle deposition, an eddy interaction model for the particle deposition has been proposed. The capacity of the model has been investigated through two test cases. The test cases of choice were a 90° bend pipe and simplified UAM. In this study, the classical EIM and that of Wang and James have also been considered for the investigation. It has been shown that the classical EIM overpredicts the particle deposition significantly, both in a simple 90° bend and in most compartments of a simplified upper airway model. The simulations from two anisotropic EIM methodologies showed better agreement in terms of both total and compartmental deposition. It was also shown that the similarity in terms of deposition results does not justify the preference of one these two anisotropic EIM methods over the other. However, of the two anisotropic EIM methods, the one we proposed here ("helicity EIM") uses three correction functions based on the computed flow field data, and does not require any priori estimation or calibration of y^+. We believe that this presents an important advantage for the simulation of respirable particles in complex geometries such as the upper airway. Here, an implicit Euler time discretization scheme, which is first order accurate, was used. The effect of time marching scheme should be investigated in future work.

Acknowledgments

This research is funded from the concerted research action (ASILUNG) grant from the Vrije Universiteit Brussels and this funding is greatly acknowledged.

References

Breuer, M., Baytekin, H.T., & Matida, E.A. (2006). Prediction of aerosol deposition in 90° bends using LES and an efficient Lagrangian tracking method. *Journal of Aerosol Science*, *37*, 1407–1428.

Brouns, M., Jayaraju, S., Lacor, C., Mey, J., Noppen, M., Vincken, W., & Verbanck, S. (2007). Tracheal stenosis: A flow dynamics study. *Journal of Applied Physiology*, *102*, 1178–1184.

Elghobashi, S. (1994). On predicting particle-laden turbulent flows. *Applied Scientific Research*, *52*, 309–329.

European Research Community on Flow Turbulence and Combustion (ERCOFTAC) (2000). Best Practice Guidelines for Computational Fluid Dynamics of Dispersed Multi-Phase Flows.

Ghorbaniasl, G., Agnihotri, V., & Lacor, C. An efficient method for the estimation of SGS model coefficient in large eddy simulation, submitted for publication.

Gosman, A.D., & Ioannides, E. (1981). Aspects of computer simulation of liquid-fuelled combustor. *AIAA Journal* 81-0323.
Graham, D.I. (1998). Improved eddy interaction models with random length and time scales. *International Journal of Multiphase flow*, *24*, 335–345.
Graham, D.I., & James, P.W. (1996). Turbulent dispersion of particles using eddy interaction models. *International Journal of Multiphase flow*, *22*, 157–175.
Grgic, B., Finlay, W.H., Burnell, P.K., & Heenan, A.F. (2004). In vitro intersubject and intrasubject deposition measurements in realistic mouth–throat geometries. *Journal of Aerosol Science*, *35*, 1025–1040.
Jayaraju, S.T., Brouns, M., Lacor, C., Belkassem, B., & Verbanck, S. (2008). Large eddy and detached eddy simulations of fluid flow and particle deposition in a human mouth–throat. *Journal of Aerosol Science*, *39*, 862–875.
Kallio, G.A., & Reeks, M.W. (1989). A numerical simulation of particle deposition in turbulent boundary layers. *International Journal of Multiphase Flow 15*, 433–446.
Kim, J., Moin, P., & Moser, R. (1987). Turbulence statistics in fully developed channel Flow at low Reynolds number. *Journal of Fluid Mechanics 177*, 133–166.
Kleinstreuer, C., & Zhang, Z. (2003). Laminar-to-turbulent fluid-particle flows in a human airway model. *Journal of Multiphase Flow*, *29*, 271–289.
Mansour, N.N., Kim, J., & Moin, P. (1988). Reynolds-stress and dissipation-rate budgets in a turbulent channel flow. *Journal of Fluid Mechanics*, *194*, 15–44.
Matida, E.A., Finlay, W.H., Breuer, M., & Lange, C.F. (2006). Improving prediction of aerosol deposition in an idealized mouth using large eddy simulation. *Journal of Aerosol Medicine*, *19*, 290–300.
Matida, E.A., Finlay, W.H., Lange, C.F., & Grgic, B. (2004). Improved numerical simulation of aerosol deposition in an idealized mouth–throat. *Journal of Aerosol Science*, *35*, 1–19.
Matida, E.A., Nishino, K., & Torii, K. (2000). Statistical simulation of particle deposition on the walls from turbulent dispersed pipe flow. *International Journal of Heat and Fluid Flow*, *21*, 389–402.
Menter, F.R. (1994). Two equation eddy-viscosity turbulence models for engineering applications. *AIAA Journal*, *32*(8), 1598–1605.
Morsi, S., & Alexander, A. (1972). An investigation of particle trajectories in two-phase flow systems. *Journal of Fluid Mechanics*, *55*, 193–208.
Pui, D.Y.H., Romay-Novas, F., & Liu, B.Y.H. (1987). Experimental study of particle deposition in bends with circular cross section. *Aerosol Science and Technology*, *7*(3), 301–315.
Sandeau, J., Katz, I., Fodil, R., Louis, B., Apiou-Sbirlea, G., Caillibotte, G., & Isabey, D. (2010). CFD simulation of particle deposition in a reconstructed human oral extrathoracic airway for air and helium–oxygen mixtures. *Journal of Aerosol Sciences*, *41*, 281–294.
Stapleton, K.W., Guentsch, E., Hoskinson, M.K., & Finlay, W.H. (2000). On the suitability of k-ε turbulence modeling for aerosol deposition in the mouth and throat: A comparison with experiment. *Journal of Aerosol Sciences*, *31*, 739–749.
Verbanck, S., Kalsi, H.S., Biddiscombe, M.F., Agnihotri, V., Belkassem, B., Lacor, C., & Usmani, O.S. (2011). Inspiratory and expiratory aerosol deposition in the upper airway. *Journal of Inhalation Toxicology*, *23*(2), 104–111.
Wang, Yi, & James, P.W. (1999). On the effect of anisotropy on the turbulent dispersion and deposition of small particles. *Journal of Multiphase Flow*, *25*, 551–558.
Zhang, Y., Finlay, W.H., & Matida, E.A. (2004). Particle deposition measurements and numerical simulation in a highly idealized mouth–throat. *Journal of Aerosol Science*, *35*, 789–803.
Zhang, Z., Kleinstreuer, C., & Kim, C.S. (2002). Micro-particle transport and deposition in a human oral airway model. *Journal of Aerosol Science*, *33*, 1635–1652.
Zhang, Z., Kleinstreuer, C., Donohue, J.F., & Kim, C.S. (2005). Comparison of micro- and nano-size particle depositions in a human upper airway model. *Journal of Aerosol Science*, *36*, 211–233.